Semi-geostrophic Flow over Orography in a Stratified Rotating Atmosphere. Part II: Some Aspects of Nonuniform Flow over an Isolated Obstacle

BRIAN D. GROSS AND WILLIAM BLUMEN*

Department of Astrophysical, Planetary, and Atmospheric Sciences, University of Colorado, Boulder, Colorado

(Manuscript received 22 October 1987, in final form 25 April 1988)

ABSTRACT

Steady, three-dimensional, inviscid flow over orography is examined by means of a semi-geostrophic model. A *nonuniform* basic current, represented by a deformation flow, is employed. A constant Coriolis parameter f and uniform potential vorticity (constant Brunt–Väisälä frequency N) characterize this model. A nondimensional mountain height $\epsilon/D \leqslant 0.5$, based on the deformation depth $D \sim 3 \times 10^3$ m, and a Rossby number $\mathrm{Ro} \leqslant 0.3$, based on the mountain breadth $L \geqslant 3.5 \times 10^5$ m, provide constraints on the flow field. Analytic solutions are represented in geostrophic coordinate space as the sum of the deformation flow and an anticyclonic mountain vortex. Although the two solutions are independent in geostrophic coordinate space, these flows are coupled nonlinearly in the transformation to physical coordinate space.

A solution is presented for flow over an isolated mountain. The decomposition of the physical space solution into fields of translation, rotation, divergence, and deformation forms the basis of the present analysis. The principal features associated with the solution are a region of relatively strong cyclonic vorticity in the lee of the mountain, accompanied by a region of convergence, and a region of weaker cyclonic vorticity on the windward slope, accompanied by a region of divergence. It is the *ageostrophic* component of the vorticity that provides these cyclonic centers, which are associated with enhanced *deformation* upstream and downstream of the peak. Further, the lee-side cyclonic vorticity enhancement is associated with *the advection of geostrophic deformation,* a feature of semi-geostrophic models that is absent in quasi-geostrophic models. By displacing the basic current's axis of dilatation into the lee of the obstacle, a deformation advection pattern is established that enhances the lee-side cyclonic vorticity center. The *uniform* flow solution is characterized by a single band of cyclonic vorticity north of the peak. This pattern is also established by the advection of geostrophic deformation. The possible relevance of the present model results to physical mechanisms that promote the initiation of lee cyclogenesis is discussed.

1. Introduction

Various analyses of airflow over orography frequently represent the upstream flow by a *uniform* basic current. For example, Merkine and Kálnay-Rivas (1976) examined steady uniform flow over isolated three-dimensional orographic features. More recently, Blumen and Gross (1987; hereafter I) extended some aspects of the Merkine and Kálnay-Rivas analysis but the specification of a uniform basic current was retained. The principal features that characterize these and other quasi-geostrophic and semi-geostrophic model solutions are a three-dimensional disturbance forced by the current flowing over the obstacle, and an anticyclonic vortex centered over the mountain peak. This vortex solution represents a steady state solution of the potential vorticity equation, and is independent of the basic flow; the properties of this latter solution have been examined by Merkine and Kálnay-Rivas and by the authors in I.

Although the use of a uniform current simplifies the mathematical analysis of orographic flow problems, this type of current is by no means the predominant one observed in the earth's atmosphere. Nonetheless, it was suggested in I that the flow pattern, essentially the superposition of the forced disturbance and the anticyclonic orographically bound vortex, may, in fact, provide a prototype flow over isolated obstacles and long ridges in some synoptic situations. An obvious failing of this model is the absence of any mechanism to maintain a cyclonic disturbance, particularly in the lee of the obstacle. Huppert and Bryan (1976) have demonstrated that the interaction between a *temporally* varying current and an isolated obstacle will be characterized by an anticyclonic eddy over the obstacle but, more importantly, cyclonic vortices also form and are observed to drift downstream. It is clear that temporal nonuniformity of the incident current in their model is essential for the generation of cyclonic vortices, while the anticyclonic bound vortex is a robust feature of

* Center for Atmospheric Theory and Analysis, University of Colorado, Boulder, Colorado.

Corresponding author address: Brian D. Gross, Dept. of Astrophysical, Planetary and Atmospheric Sciences, University of Colorado, Boulder, CO 80309.

steady and nonsteady flows, and is related to the vertical compression of vortex tubes, e.g., Smith (1979).

However, observed flows also exhibit *spatial* nonuniformity. For example, two instances of a synoptic-scale diffluent flow incident on the Alps are shown in Fig. 1. The configuration in Fig. 1a arises from the juxtaposition of a trough of low pressure to the northeast of the Alps, and an anticyclone to the northwest, while in Fig. 1b the anticyclone is southwest of the Alps. In these examples, prominent flow diffluence is clearly established by the large-scale weather patterns far from the Alps.

The present study retains the steady, uniform potential vorticity semi-geostrophic model used in I, but the basic current flowing over the orography is nonuniform: it is represented by a deformation flow. The steady solution is not just the superposition of this deformation flow and the anticyclonic vortex. The two flows are coupled, and the relative importance of this inherent nonlinearity will be examined.

The vortex solution, associated with either a quasi-geostrophic or a semi-geostrophic model, provides a characteristic anticyclonic relative vorticity pattern directly over the obstacle, surrounded by relatively weak cyclonic vorticity. However, a semi-geostrophic model, in which the flow is represented by both an anticyclonic vortex and a deformation pattern, contains the essential elements to establish a relatively pronounced lee-side cyclonic vorticity center accompanied by a convergent flow pattern. This circumstance arises because two cyclonic vorticity centers emerge in the ageostrophic vorticity field: they are symmetrically placed on the windward and leeward slopes. Most importantly, the cyclonic vorticity in the lee is enhanced in a *semi-geostrophic* model by placing the dilatation axis of the deformation flow on the leeward slope. Flow asymmetry is accomplished by including advection *by* the ageostrophic flow in the semi-geostrophic model, a feature not contained in a quasi-geostrophic model.

Prominent deformation flows of the type shown in Fig. 1 are often established prior to cyclogenesis events in the Alpine region. It is clear that the steady, semi-geostrophic, uniform potential vorticity model could not be expected to contain all essential elements that characterize lee cyclogenesis. For example, the advection *of* ageostrophic flow may not be negligible, and the developmental process itself is beyond the scope of the present investigation. The goal of this study is to isolate physical processes, particularly those not adequately treated by a quasi-geostrophic model, that could be instrumental in establishing a favorable environment for further cyclonic development.

The basic model and method of solution are presented in section 2. A discussion of the transformation from geostrophic coordinate space to physical coordinate space is presented in section 3. Analytic solutions for an isolated mountain are presented in section 4. The possible relevance of the physical processes revealed by these solutions to the problem of lee cyclogenesis is discussed in section 5.

2. Model

The steady model used in I is adopted here. A basic current flows over an isolated mountain $h(x, y)$. The flow is inviscid, hydrostatic, and adiabatic. It possesses constant potential vorticity, and is characterized by both a constant Brunt–Väisälä frequency and constant Coriolis parameter f. There is only one difference between the present model and the one used in I: the basic current that flows over the orography is nonuniform, with spatial variability in the horizontal plane.

The geostrophic coordinates (X, Y, Z), directed in the eastward, northward, and vertical directions respectively, are introduced. They are defined by

$$\left.\begin{aligned} X &= x + \mathrm{Ro} v_g(x, y, z) \\ Y &= y - \mathrm{Ro} u_g(x, y, z) \\ Z &= z \end{aligned}\right\} \tag{1}$$

where (x, y, z) represent physical space coordinates. The analysis is carried out in geostrophic coordinate space (X, Y, Z), and the flow fields are transformed to physical coordinate space (x, y, z) by means of (1). The geostrophic velocities are given by

$$u_g = -\frac{\partial \Phi}{\partial Y} \tag{2}$$

$$v_g = \frac{\partial \Phi}{\partial X}, \tag{3}$$

and the potential temperature is

$$\Theta(Z) + \theta(X, Y, Z) = Z + \mathrm{Ro}\,\frac{\partial \Phi}{\partial Z}, \tag{4}$$

where Φ represents the geopotential in geostrophic coordinate space. The Rossby number $\mathrm{Ro} = U/fL$ is based on a characteristic horizontal velocity scale U and the mountain breadth L.

The geostrophic streamfunction Φ satisfies Laplace's equation,

$$\left[\frac{\partial^2}{\partial X^2} + \frac{\partial^2}{\partial Y^2} + \frac{\partial^2}{\partial Z^2}\right]\Phi = 0, \tag{5}$$

when relatively small quadratic terms are neglected. The justification for neglecting these latter terms is discussed in the Appendix. An isentropic lower boundary is prescribed by

$$Z + \mathrm{Ro}\,\frac{\partial \Phi}{\partial Z} = Z_0, \quad Z = h(X, Y) \tag{6}$$

where Z_0 is the level surface both upstream and downstream of the mountain or, equivalently, the uniform

potential temperature of the lower boundary. The ageostrophic velocity components (u_a, v_a, w), obtained from the semi-geostrophic model equations employed in I, are

$$\mathrm{Ro}u_a = -\mathrm{Ro}^2\left[u_g\frac{\partial}{\partial X} + v_g\frac{\partial}{\partial Y} + w\frac{\partial}{\partial Z}\right]v_g, \tag{7}$$

$$\mathrm{Ro}v_a = \mathrm{Ro}^2\left[u_g\frac{\partial}{\partial X} + v_g\frac{\partial}{\partial Y} + w\frac{\partial}{\partial Z}\right]u_g, \tag{8}$$

$$\mathrm{Ro}w = -\mathrm{Ro}^2\left[u_g\frac{\partial\theta}{\partial X} + v_g\frac{\partial\theta}{\partial Y}\right]\Big/\left(1 + \frac{\partial\theta}{\partial Z}\right). \tag{9}$$

A basic state deformation flow of strength α that satisfies (5) and (6) is given by

$$\mathrm{Ro}\bar{\Phi} = \alpha\left[XY\cos(2\beta) + \tfrac{1}{2}(X^2 - Y^2)\sin(2\beta)\right], \tag{10}$$

where the axis of contraction is rotated clockwise by an angle β from the east–west axis. Since this particular solution of Laplace's equation is independent of Z, the basic flow (10) does not contribute to the potential temperature in (4) nor to the geostrophic coordinate representation of the lower boundary in (6). The geostrophic velocities associated with the basic current (10) are

$$\mathrm{Ro}\bar{u}_g = \alpha(Y\sin2\beta - X\cos2\beta), \tag{11}$$

$$\mathrm{Ro}\bar{v}_g = \alpha(Y\cos2\beta + X\sin2\beta), \tag{12}$$

and this flow is irrotational in geostrophic coordinate space.

The anticyclonic mountain vortex solution, introduced in I, also satisfies (5) and (6). This solution is expressed by

$$\mathrm{Ro}\Phi' = \mu^3\left(\frac{1+a}{a}\right)\ln\left(\frac{\zeta+1}{\zeta-1}\right) - \mu^3\ln[1 + (a/2)^2], \tag{13}$$

where

$$\left.\begin{aligned}\zeta &= (r_1 + r_2)/a\\ r_1 &= [X^2 + Z^2 + (Y + a/2)^2]^{1/2}\\ r_2 &= [X^2 + Z^2 + (Y - a/2)^2]^{1/2}\end{aligned}\right\}, \tag{14}$$

μ^3 is a constant, and the parameter a represents a measure of the length to the breadth of the mountain. The geostrophic streamfunction (13) associated with the mountain vortex decays to zero as $(|X|, |Y|, Z) \to \infty$. Interactions between the deformation flow (10) and the vortex circulation (13) appear when the geostrophic coordinate space solution is transformed to physical space by means of (1). This type of interaction does not appear when the basic flow is represented by a uniform current.

The basis of selection of the deformation strength α, the mountain height ϵ (or equivalently, the vortex strength μ), and the Rossby number Ro, are discussed in the Appendix. Values in the present study are

$$\left.\begin{aligned}\alpha &= 0.2\\ \epsilon/D &= 0.5\\ \mathrm{Ro} &= 0.3\end{aligned}\right\}. \tag{15}$$

In an atmosphere characterized by a deformation depth $D \sim 3 \times 10^3$ m, the mountain height is $\epsilon \sim 1.5 \times 10^3$ m. The Rossby number in (15) represents, for example, a midlatitude flow of characteristic magnitude $U \sim 10$ m s^{-1} incident on a mountain with half-width $L \sim 333 \times 10^3$ m.

3. The coordinate transformation

Flow over an isolated mountain, which has a circular planform in geostrophic coordinate space, is considered. This shape, also considered in I, may be obtained from (6) and (13) in the limiting case $a \to 0$. The geostrophic streamfield of the basic barotropic current, which does not contribute to (6), is given by (10) with $\beta = 45°$. In this limit, the total geostrophic streamfunction reduces to the sum of a shearing deformation flow and an axisymmetric vortex,

$$\mathrm{Ro}(\bar{\Phi} + \Phi) = \frac{\alpha}{2}(X^2 - Y^2) + \frac{\mu^3}{[(X - X_0)^2 + (Y - Y_0)^2 + Z^2]^{1/2}}, \tag{16}$$

where the prime notation introduced in (13) will now be dropped. The location of the mountain peak is at (X_0, Y_0) in geostrophic coordinates. The geostrophic velocities associated with the solution (16) are given by

$$\mathrm{Ro}(\bar{u}_g + u_g) = \alpha Y + \frac{\mu^3(Y - Y_0)}{[(X - X_0)^2 + (Y - Y_0)^2 + Z^2]^{3/2}}, \tag{17a}$$

$$\mathrm{Ro}(\bar{v}_g + v_g) = \alpha X - \frac{\mu^3(X - X_0)}{[(X - X_0)^2 + (Y - Y_0)^2 + Z^2]^{3/2}}. \tag{17b}$$

The disturbance associated with the mountain decays vertically within a deformation depth ($D \sim 3 \times 10^3$ m) of the mountain. Consequently, the present discussion will be limited to flow along the lower boundary, where the disturbance is most pronounced.

The notation

$$\delta = \frac{\mu^3}{[(X - X_0)^2 + (Y - Y_0)^2 + Z^2]^{3/2}} \tag{18}$$

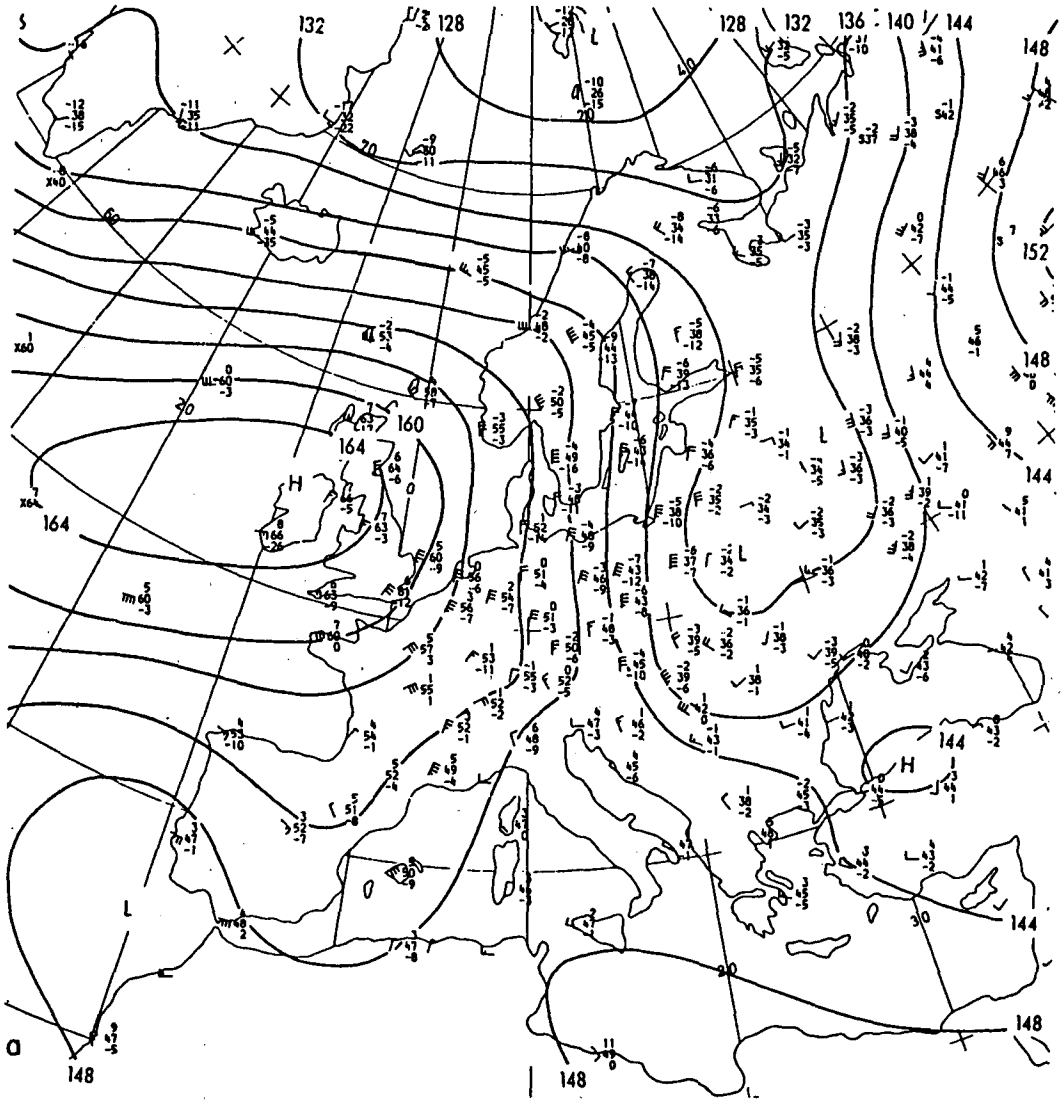

FIG. 1. Examples of a deformation flow incident on the Alps. The center of the Alps is located approximately at 47°N 10°E. (a) The 850 mb analysis of geopotential height (in decameters) at 0000 UTC 27 April 1982. (b) As in (a), except on 2 March 1982. A cyclone developed in the lee of the Alps 1 day later. (Reprinted from the European Meteorological Bulletin, ISSN 0341-2970.)

is now introduced. Then the expression in (6) may be used with (16) and (18) to show that

$$\delta = \frac{h(X, Y)}{Z_0 + h(X, Y)} \leqslant 0.5 \tag{19}$$

remains constant along height contours on the lower boundary. The geostrophic velocity in (17) may now be expressed as

$$\mathrm{Ro}(\bar{u}_g + u_g) = \alpha Y + \delta(Y - Y_0), \tag{20a}$$

$$\mathrm{Ro}(\bar{v}_g + v_g) = \alpha X - \delta(X - X_0), \tag{20b}$$

and the geostrophic coordinates (1) evaluated along the lower boundary are

$$X = x + \alpha X - \delta(X - X_0), \tag{21a}$$

$$Y = y - \alpha Y - \delta(Y - Y_0). \tag{21b}$$

Evaluation of (21a, b) at the mountain peak yields

$$x_0 = (1 - \alpha)X_0, \tag{22a}$$

$$y_0 = (1 + \alpha)Y_0, \tag{22b}$$

where (x_0, y_0) are the coordinates of the mountain peak in physical space. Solving (21a, b) for the physical coordinates yields

$$x - x_0 = (1 + \delta - \alpha)(X - X_0), \tag{23a}$$

$$y - y_0 = (1 + \delta + \alpha)(Y - Y_0). \tag{23b}$$

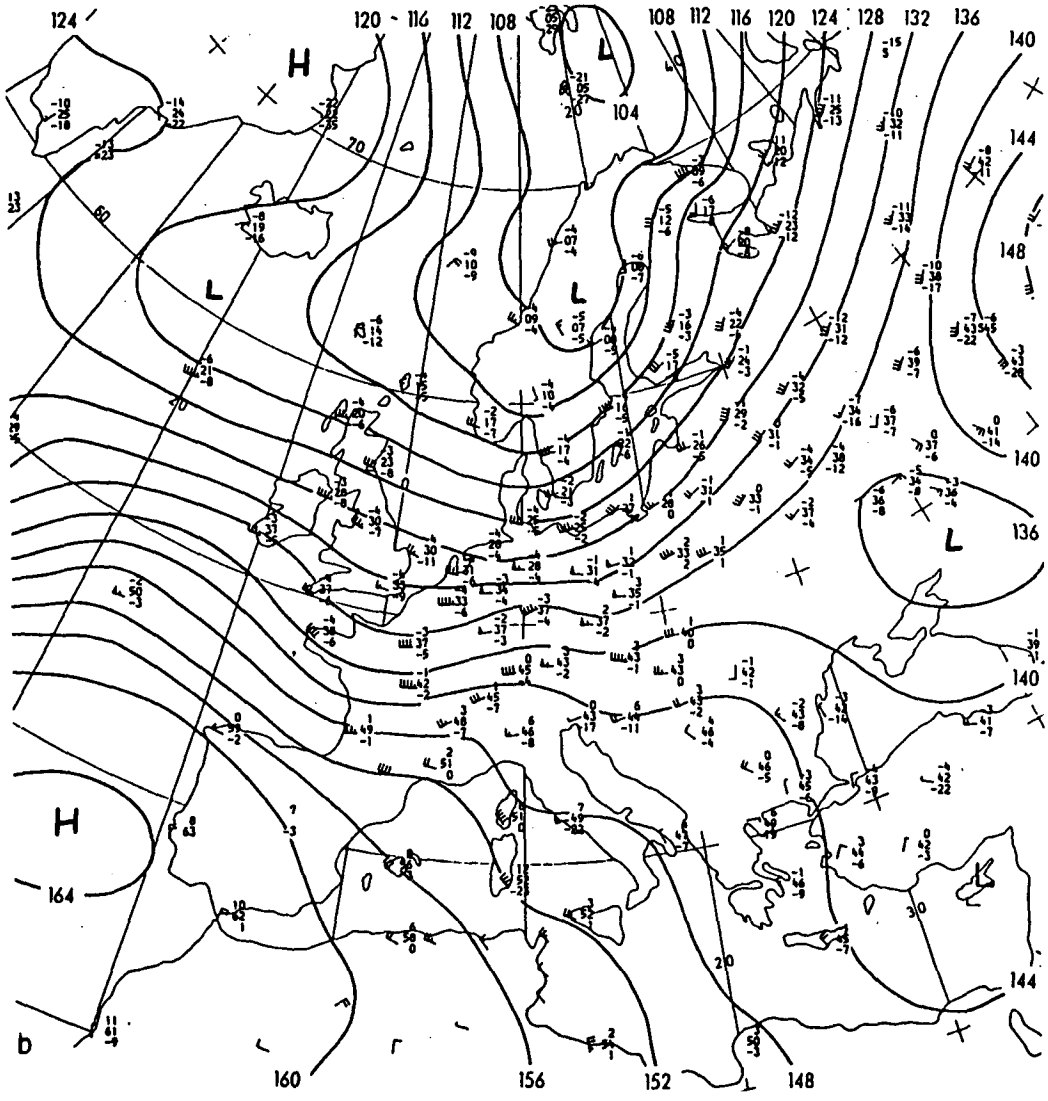

FIG. 1. (*Continued*)

Horizontal distances from the mountain peak in physical space are expressed in (23a, b) in terms of horizontal distances from the mountain peak in geostrophic space.

The transformation (23) from geostrophic to physical coordinate space introduces a distortion of the flow variables and the mountain shape. This distortion may be examined by considering a circular contour, with its center at the peak, given in geostrophic coordinates by

$$X^2 + Y^2 = C^2, \tag{24}$$

where C is a constant and $X_0 = Y_0 = 0$ for simplicity. With the coordinate transformation (23), (24) may be written as

$$\frac{x^2}{(1+\delta-\alpha)^2} + \frac{y^2}{(1+\delta+\alpha)^2} = C^2. \tag{25}$$

This is an equation for an ellipse in physical coordinate space, located along the lower boundary and centered on the peak, with the major axis oriented in the north–south direction. The circle (24) and the ellipse (25), corresponding to the mountain half-width contour ($\delta = 0.27$, $C = 1$), are shown in Fig. 2. The ratio of the major to minor axes of the ellipse is given by

$$r = \frac{(1+\delta+\alpha)}{(1+\delta-\alpha)}, \tag{26}$$

and this ratio is $r \approx 1.4$ for the ellipse shown in Fig. 2. The area encompassed by an arbitrary height contour of the elliptic mountain is given by

$$A = \pi C^2[(1+\delta)^2 - \alpha^2], \tag{27}$$

which may be greater than or less than the area πC^2 of the original circular contour, depending on the value

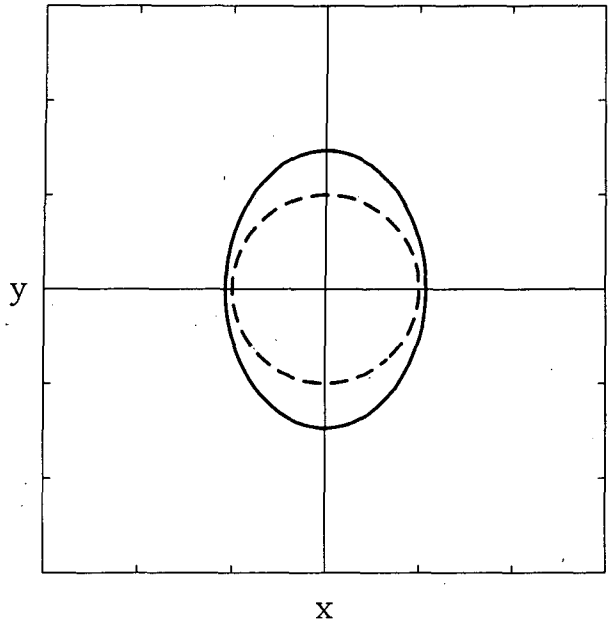

FIG. 2. The circle given in (24) and the ellipse given in (25), corresponding to the mountain half-width contour ($\delta = 0.27$, $C = 1$). Tick marks indicate horizontal distance, in units of mountain half-widths in geostrophic space.

of δ associated with that contour. The area of the ellipse shown in Fig. 2 is $A \approx 1.6\pi C^2$.

The effects of the coordinate transformation are illustrated in Fig. 3, where the vertical component of geostrophic vorticity on the lower boundary has been plotted in both geostrophic and physical coordinate space, along the axes shown in Fig. 2. In this semi-geostrophic model, the vorticity in *physical* coordinate space is defined by

$$\zeta_g = \frac{\mathrm{Ro}\nabla_H^2(\bar{\Phi} + \Phi)}{1 - \mathrm{Ro}\nabla_H^2(\bar{\Phi} + \Phi)}, \tag{28}$$

where $\mathrm{Ro}\nabla_H^2(\bar{\Phi} + \Phi)$, the horizontal Laplacian of the geostrophic streamfunction, represents the vertical component of geostrophic vorticity in *geostrophic* coordinate space (Hoskins 1975). The strength of the mountain anticyclone is approximately halved in the transformation from geostrophic to physical coordinate space, according to (28). Further, the coordinate transformation considerably broadens the mountain anticyclone along the north–south axis, as shown in Fig. 3a. This latter effect is a consequence of coordinate stretching by both the mountain vortex and the deformation flow in (23b). However, as shown in Fig. 3b, there is no appreciable change in the east–west breadth of the anticyclone: coordinate stretching by the mountain vortex is offset by coordinate compression by the deformation flow in the coordinate transformation (23a). These effects of the coordinate transformation are also evident in the distortion of the mountain half-width contour shown in Fig. 2.

4. Flow characteristics

The geostrophic velocity in (20) may be expressed in physical coordinates with the aid of (23a, b) as

$$\mathrm{Ro}(\bar{u}_g + u_g) = \frac{\alpha + \delta}{1 + \delta + \alpha}(y - y_0) + \frac{\alpha y_0}{1 + \alpha}, \tag{29a}$$

$$\mathrm{Ro}(\bar{v}_g + v_g) = \frac{\alpha - \delta}{1 + \delta - \alpha}(x + x_0) + \frac{\alpha x_0}{1 - \alpha}. \tag{29b}$$

The first set of terms on the right-hand side of (29) represents the total geostrophic flow, for a deformation flow centered on the mountain peak at (x_0, y_0). The addition of a uniform velocity, represented by the last set of terms in (29), displaces the deformation flow center away from the mountain peak. The geostrophic streamfunction associated with the velocity (29) is shown in Fig. 4.

The geostrophic flow (29) may be conveniently resolved into four types of motion (Petterssen 1953). Translation is represented by the constant velocity component in (29). The horizontal divergence, given by

$$d = \frac{\partial u}{\partial x} + \frac{\partial v}{\partial y}, \tag{30}$$

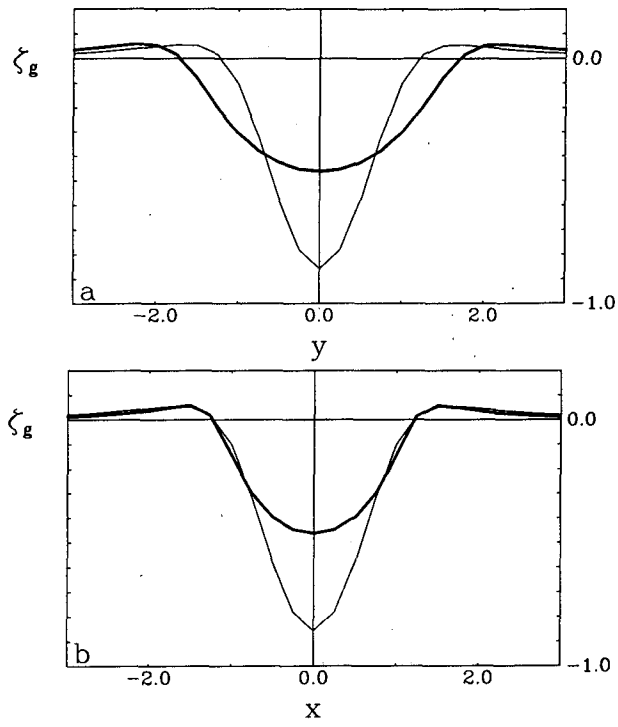

FIG. 3. Vertical component of geostrophic vorticity. (a) North–south cross section along the $X = X_0$ axis in geostrophic space (thin line) and along the $x = x_0$ axis in physical coordinate space (heavy line). (b) East–west cross section along the $Y = Y_0$ axis in geostrophic coordinate space (thin line) and along the $y = y_0$ axis in physical coordinate space (heavy line). Tick marks along the abscissa indicate horizontal distance, in units of east–west half-widths.

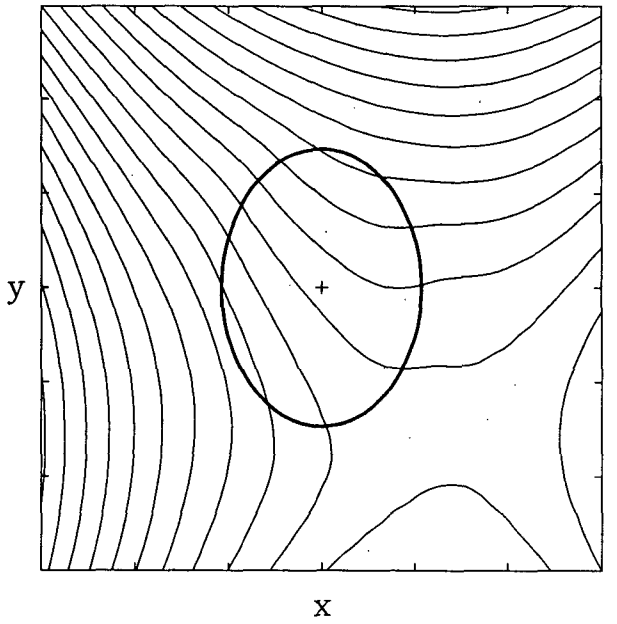

FIG. 4. Geostrophic stream field along the lower boundary of an isolated mountain. The heavy closed contour is the height contour corresponding to the mountain half-width. The peak is at $(X_0, Y_0) = (-1.4, 1.4)$, so that the deformation flow center is located two half-widths southeast of the peak in geostrophic coordinate space. Tick marks indicate horizontal distance, in units of mountain half-widths.

vanishes for the geostrophic flow (29). The rotational component of the flow is represented by the vertical component of vorticity, which is given by

$$\zeta = \frac{\partial v}{\partial x} - \frac{\partial u}{\partial y}. \tag{31}$$

The geostrophic vorticity ζ_g associated with the flow expressed by (29) is shown in Fig. 5. The principal feature in this vorticity distribution is the mountain anticyclone, with magnitude $0.5f$, which has been discussed in detail by Merkine and Kálnay-Rivas (1976) and by the authors in I. Relatively weak cyclonic vorticity (outside the zero contour in Fig. 5) is associated with the monotonic decay of this anticyclonic vortex outside of the mountain half-width (see Fig. 3).

The deformational component of the flow is represented by the shearing and stretching deformation, which are given respectively by

$$\eta = \frac{\partial v}{\partial x} + \frac{\partial u}{\partial y}, \tag{32}$$

$$\tau = \frac{\partial u}{\partial x} - \frac{\partial v}{\partial y}. \tag{33}$$

The geostrophic components of the deformation associated with (29) are shown in Fig. 6. These distributions form the basis for the discussion below. A fundamental quantity, that is independent of a rotation of the coordinate axes, is the total deformation, defined by

$$\gamma = \sqrt{\eta^2 + \tau^2}. \tag{34}$$

The total geostrophic deformation γ_g associated with (29) is shown in Fig. 7. A comparison of this deformation distribution and the geostrophic vorticity distribution shown in Fig. 5 reveals that the deformation is much greater than the cyclonic vorticity at levels below the mountain half-width, where the vortex starts to weaken. Therefore, deformation, rather than cyclonic vorticity, characterizes the flow as the mountain anticyclone decays away from the peak. (The deformation associated with the basic flow (10) is constant, and is given by $2\alpha/(1 - \alpha^2) = 4.2 \times 10^{-5}\ s^{-1}$ when $\alpha = 2 \times 10^{-5}\ s^{-1}$.)

The deformation exhibited in Fig. 7 is largest east and west of the peak, where the magnitude is about $8 \times 10^{-5}\ s^{-1}$. This feature is associated with the *shearing* deformation distribution shown in Fig. 6a. East and west of the peak, the shear of the basic deformation flow and the shear associated with the decay of the mountain vortex are both cyclonic, i.e., $\partial \bar{v}_g/\partial x > 0$ and $\partial v_g/\partial x > 0$. In contrast, north and south of the peak, the shear of the basic flow is anticyclonic ($\partial \bar{u}_g/\partial y > 0$), and the shear of the vortex is cyclonic ($\partial u_g/\partial y < 0$), so that the total shearing deformation is much less in these regions: the magnitude there is about $10^{-5}\ s^{-1}$. The deformation distribution associated with the vortex alone is shown in Fig. 8. Clearly, no contribution

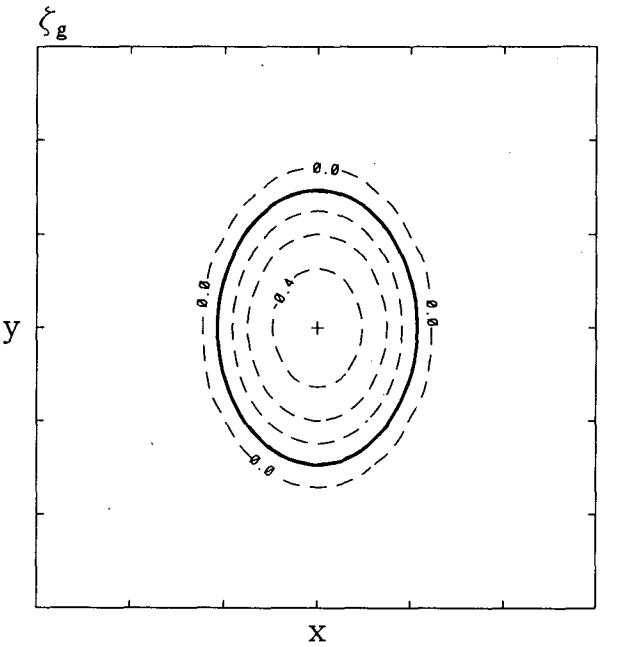

FIG. 5. The vertical component of geostrophic vorticity. Dashed lines are contours of anticyclonic vorticity. The minimum value is $-4.5 \times 10^{-5}\ s^{-1}$. The contour interval is $1 \times 10^{-5}\ s^{-1}$. The heavy closed contour is the height contour corresponding to the mountain half-width.

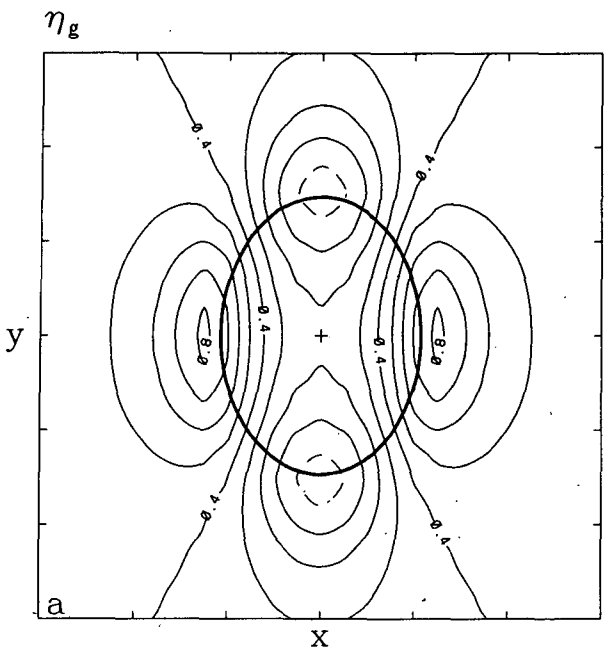

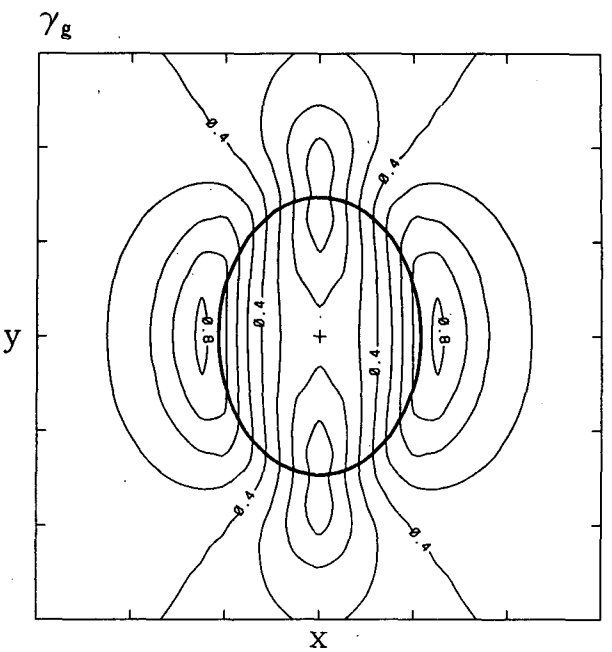

FIG. 7. As in Fig. 6, except the total geostrophic deformation, γ_g. The maximum and minimum values are 8×10^{-5} and 1×10^{-5} s^{-1}.

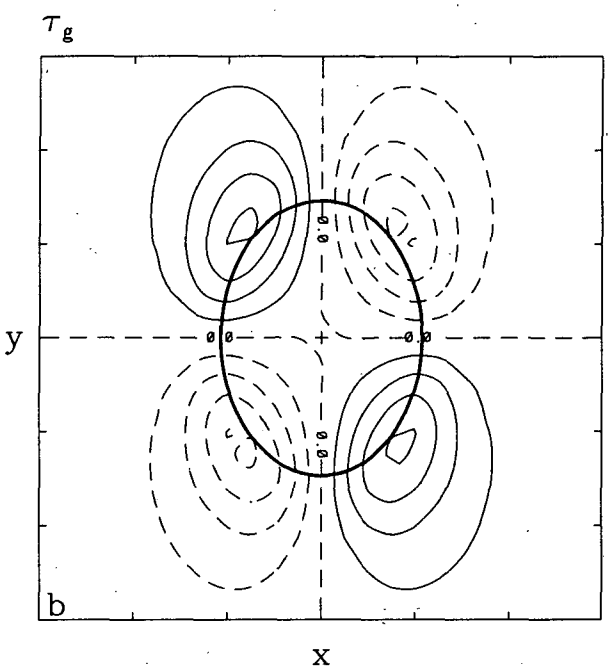

FIG. 6. The geostrophic (a) shearing deformation and (b) stretching deformation. Dashed lines indicate negative values. The contour interval is 1×10^{-5} s^{-1}. The heavy closed contour is the height contour corresponding to the mountain half-width.

to the deformation is made by a uniform basic flow. Consequently, the solution associated with a uniform flow does not possess the characteristic features illustrated in Fig. 7.

Petterssen (1953) has shown that the geostrophic vorticity, shown in Fig. 5, may not provide a good approximation to the total vorticity: the *ageostrophic* vorticity may provide a significant contribution as well. In fact, he showed that only in straight, nondivergent

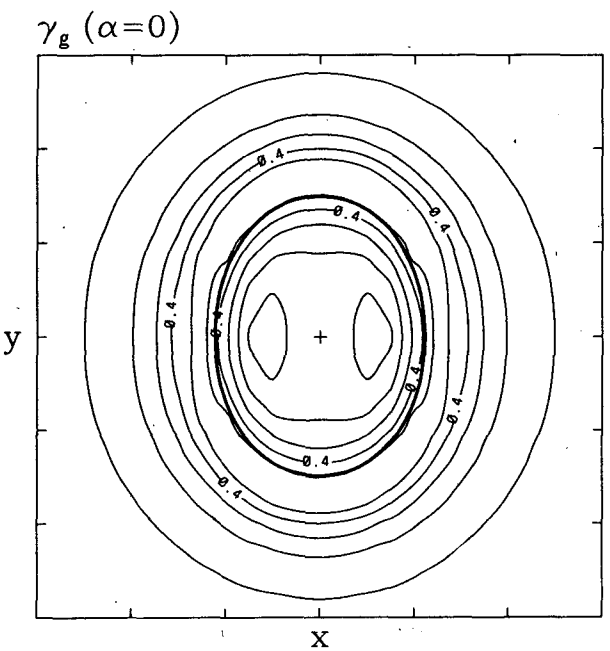

FIG. 8. As in Fig. 4, except the total geostrophic deformation corresponding to *uniform* flow over an isolated mountain. The maximum and minimum values are 5.5×10^{-5} and 1×10^{-5} s^{-1}.

flow with lateral shear is the total vorticity accurately represented by the geostrophic vorticity. Otherwise, an ageostrophic contribution to the vorticity, associated with centripetal accelerations and accelerations associated with confluence and diffluence in the flow (Sherman 1952), is present when the geopotential field possesses both curvature and diffluence. In general, such curvature and diffluence will exist in the flow, as is the case shown in Fig. 4. Here, the geostrophic vorticity is symmetric about the mountain peak (see Fig. 5), and any asymmetry in the vorticity field must be associated with the ageostrophic component. This contribution is necessarily smaller than the geostrophic field, since both flow curvature and changes in the wind speed along the flow must be relatively small in the geostrophic momentum approximation (Hoskins 1975).

The nondimensional ageostrophic vertical component of vorticity, the horizontal divergence, and the ageostrophic shearing and stretching deformations are given by

$$\zeta_a \approx \frac{\gamma_g^2 - \zeta_g^2}{2 + \zeta_g} + \frac{\tau_g \tau_a + \eta_g \eta_a}{2 + \zeta_g} \tag{35}$$

$$d_a \approx -\frac{2}{2 + \zeta_g} \frac{D\zeta_g}{Dt} + \frac{\tau_g \eta_a - \eta_g \tau_a}{2 + \zeta_g} \tag{36}$$

$$\eta_a \approx \frac{2}{2 + \zeta_g} \frac{D\tau_g}{Dt} + \frac{\tau_g d_a + \eta_g \zeta_a}{2 + \zeta_g} \tag{37}$$

$$\tau_a \approx -\frac{2}{2 + \zeta_g} \frac{D\eta_g}{Dt} + \frac{\tau_g \zeta_a - \eta_g d_a}{2 + \zeta_g} \tag{38}$$

where the subscripts g and a denote geostrophic and ageostrophic values of the quantities defined in (30)–(33), and products of ageostrophic quantities are neglected under the constraint of the geostrophic momentum approximation. In addition, small terms proportional to horizontal derivatives of the vertical velocity have been neglected for purposes of discussion (although they are retained in the numerical evaluations of the solution), and

$$\frac{D}{Dt} = (\bar{u}_g + u_g + u_a) \frac{\partial}{\partial x} + (\bar{v}_g + v_g + v_a) \frac{\partial}{\partial y} + w \frac{\partial}{\partial z}. \tag{39}$$

The distributions of the quantities in (35)–(38) are shown in Fig. 9.

It is apparent from the ageostrophic distributions of (ζ_a, d_a, η_a, τ_a) that asymmetries are introduced into the total fields by the ageostrophic flow. The principal features in the vorticity distribution shown in Fig. 9a are a region of relatively strong cyclonic vorticity in the lee of the mountain, with a magnitude of about $0.55f$, and a weaker region of cyclonic vorticity on the windward slope, with a magnitude of about $0.4f$. Examination of (35) and the total geostrophic deformation γ_g shown in Fig. 7 reveals that the ageostrophic cyclonic vorticity centers arise primarily from the dependence of ζ_a on the geostrophic deformation γ_g: the regions of cyclonic ageostrophic vorticity in Fig. 9a coincide with those of enhanced deformation in Fig. 7. In fact, (35) may be expressed to leading order as

$$\zeta_a \approx \frac{\gamma_g^2 - \zeta_g^2}{2} \tag{40}$$

which is formally the ageostrophic relationship, corresponding to (35), in a *quasi-geostrophic* model. When the deformation γ_g is negligible compared to the vorticity ζ_g in (40), the ageostrophic vorticity represents an anticyclonic correction to the geostrophic vorticity, which by itself overestimates cyclonic vorticity and underestimates anticyclonic vorticity in a curved, divergent geopotential field (Petterssen 1953). It is precisely this anticyclonic ageostrophic flow ($\zeta_a \approx -\zeta_g^2/2$) that provides the gradient wind correction to the circular vortex solution that has been examined in I.

The leading order contributions to the ageostrophic vorticity (40), namely the geostrophic deformation shown in Fig. 7 and the geostrophic vorticity shown in Fig. 5, provide a symmetric distribution of cyclonic vorticity, as shown in Fig. 10. Consequently, the *asymmetry* of the vorticity distribution shown in Fig. 9a arises from the contribution by the ageostrophic shearing and stretching deformations that appear in (35) and are shown in Fig. 9b and Fig. 9c. This contribution may be expressed to leading order as

$$\frac{\tau_g \tau_a + \eta_g \eta_a}{2 + \zeta_g} \approx -\frac{1}{2}\left(\tau_g \frac{D\eta_g}{Dt} - \eta_g \frac{D\tau_g}{Dt}\right), \tag{41}$$

where D/Dt is given by (39). A comparison of the total ageostrophic vorticity shown in Fig. 9a with the leading order contribution shown in Fig. 10 reveals that the contribution (41) enhances the ageostrophic cyclonic vorticity in the lee of the mountain, and diminishes it on the windward slope, for the basic flow shown in Fig. 4.

In the *uniform* flow solution, the ageostrophic vorticity distribution consists of a banded region of cyclonic vorticity that bends around the obstacle north of the peak, as shown in Fig. 11a. The vorticity provided by the leading order term of (35), expressed by (40), is nearly symmetric about the peak, as shown in Fig. 11b. This distribution does not exhibit the cyclonic vorticity centers shown in Fig. 10, because there is no contribution by the uniform flow to either the geostrophic shearing deformation η_g or the geostrophic stretching deformation τ_g. In this case, the contribution (41) provides an asymmetrical vorticity pattern, *but it is a single banded structure, rather than two distinct vorticity centers,* that emerges in Fig. 11a.

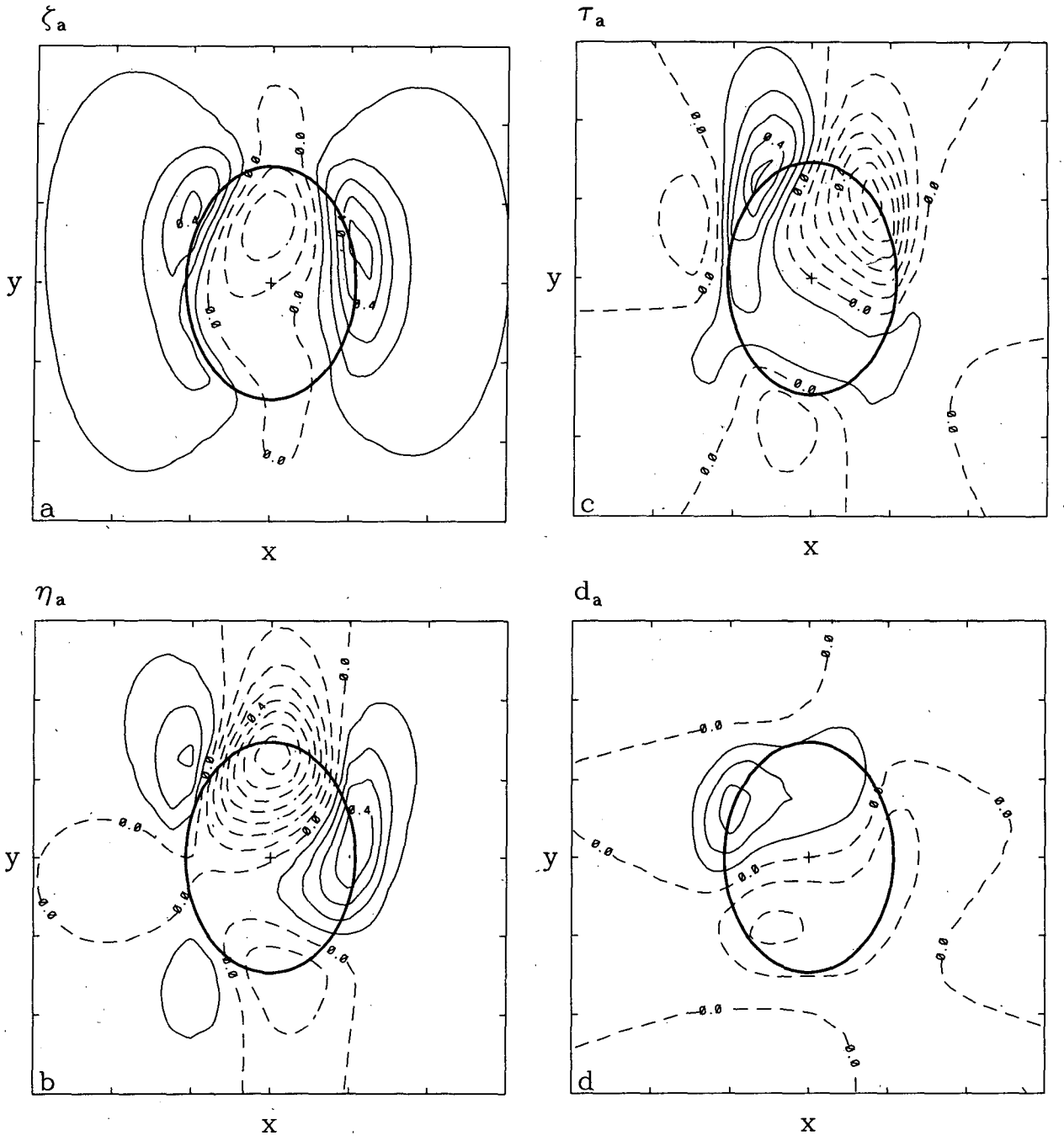

FIG. 9. The ageostrophic (a) vertical component of vorticity, with a magnitude of about 5.5×10^{-5} s^{-1} on the lee slope and 4×10^{-5} s^{-1} on the windward slope, (b) shearing deformation, (c) stretching deformation, (d) divergence, with a magnitude of about 3×10^{-5} s^{-1} on the windward slope, and -2×10^{-5} s^{-1}, corresponding to convergence, in the lee. Dashed lines represent negative values. The contour interval is 1×10^{-5} s^{-1}. The heavy closed contour is the height contour corresponding to the mountain half-width.

The principal features in the distribution of horizontal divergence, shown in Fig. 9d, are a broad region of convergence in the lee, with a magnitude of about $0.2f$, and a region of divergence on the windward slope, with a magnitude of about $0.3f$. This distribution arises primarily from the advection of geostrophic vorticity. The ageostrophic divergence (36) may be expressed to leading order as

$$d_a \approx -\frac{D\zeta_g}{Dt}. \tag{42}$$

In particular, the relatively compact field of divergence

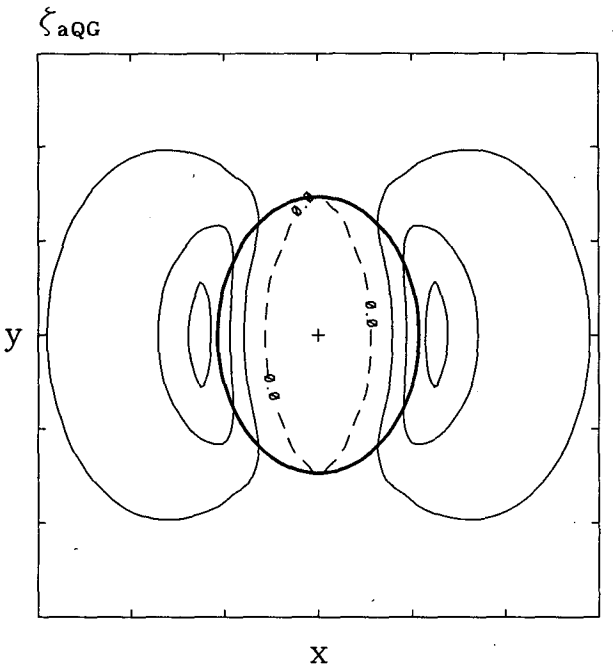

FIG. 10. The leading order contributions to the ageostrophic vorticity expressed in (40), corresponding to the *quasi-geostrophic* distribution. Dashed lines represent negative values. The maximum and minimum values are 3×10^{-5} and -0.5×10^{-5} s^{-1}. The contour interval is 1×10^{-5} s^{-1}. The heavy closed contour is the height contour corresponding to the mountain half-width.

on the windward slope in Fig. 9d may be associated with vorticity advection from the northwest quadrant (see Fig. 4) toward the mountain anticyclone center. The broader field of convergence in the lee arises from weaker advection on the leeward side of the mountain anticyclone. The asymmetry in the strength of the advecting flow arises from the displacement of the deformation flow center into the lee of the mountain. Clearly, no such asymmetry in the wind speed exists in a uniform flow solution, and the divergence pattern given by (42) would be exactly antisymmetric about the mountain peak, with divergence on the windward slope and convergence in the lee.

A comparison of Figs. 9a and 9d reveals that the contours of divergence and cyclonic vorticity overlap each other on the windward slope. This type of distribution would tend to weaken cyclonic vorticity in a time-dependent model. However, the lee-side distribution of cyclonic vorticity is embedded in a broad region of flow convergence, which is conducive to further enhancement of the vorticity.

5. Conclusion

A relatively simple semi-geostrophic solution has been presented that represents deformation flow over an isolated obstacle. This solution clearly exposes the respective roles of the nonuniform basic state, the mountain vortex, and the position of the mountain with respect to the deformation axes, in producing the structure of the circulation features in physical space that are displayed in Figs. 5–7 and Fig. 9. This study has demonstrated that spatial nonuniformity in the basic current can provide a mechanism for the gen-

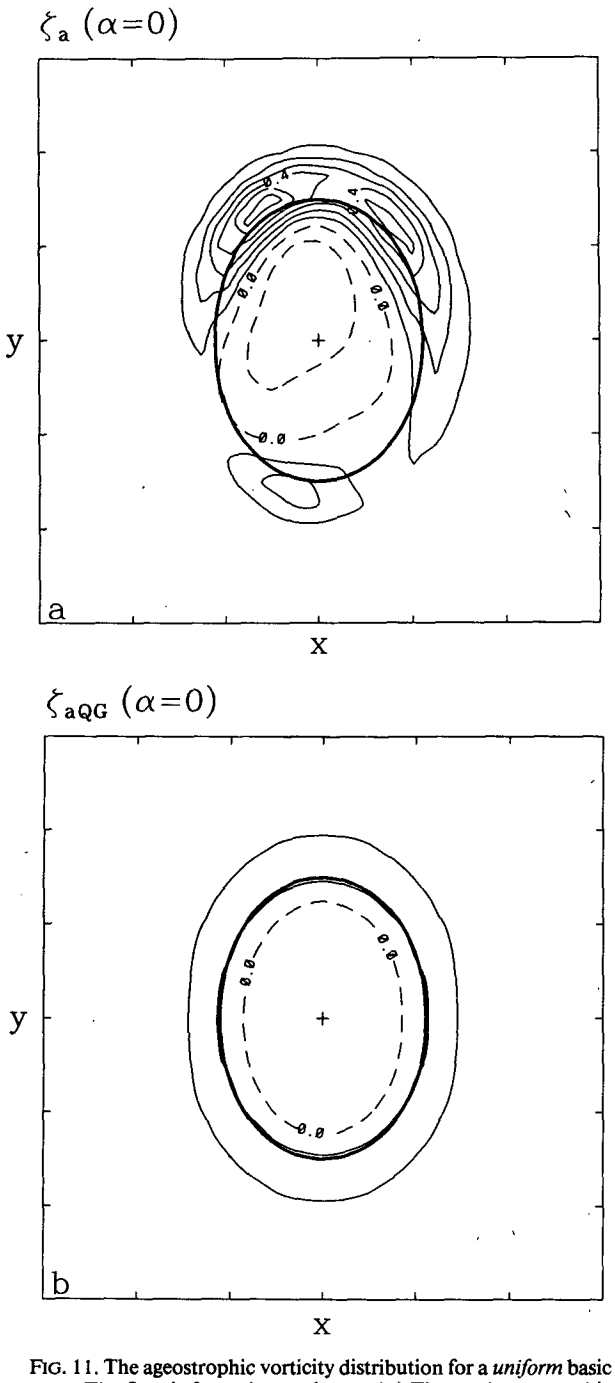

FIG. 11. The ageostrophic vorticity distribution for a *uniform* basic current. The flow is from the northwest. (a) The total ageostrophic vorticity expressed in (35). The maximum and minimum values are 6×10^{-5} and -1.5×10^{-5} s^{-1}. (b) The leading order contributions to the ageostrophic vorticity expressed in (40), corresponding to the *quasi-geostrophic* distribution. The contour interval is 1×10^{-5} s^{-1}.

eration of a cyclonic vorticity center with a magnitude of about $0.5f$, accompanied by convergence, in the lee of an isolated mountain.

It is clear that there are various limitations that would restrict the application of these results to physical processes in the atmosphere, such as cyclogenesis in the lee of mountains. The restriction to steady, uniform potential vorticity flow has been noted in the Introduction. Clearly, the roles of friction and diabatic heating in the formation of lee cyclones needs to be resolved. The intention here has been to isolate dynamical processes that may be associated with confluent and diffluent flows over isolated mountains.

It may be argued that the steady bound vortex solution may not be a robust property of orographic flows. Certainly, Merkine and Kálnay-Rivas (1976) have noted that the initial-value problem needs to be examined to establish the conditions for its existence. However, the authors in I have noted that this bound vortex has often been observed over sea mounts. In addition, its presence in atmospheric flows over mountainous terrain cannot be overruled, as indicated in the model solutions presented in I. It is on this basis that the present results may provide some physical insights into the formative stages of lee cyclogenesis.

Both Radinović (1986) and McGinley (1982) have proposed theories of lee cyclogenesis that require the presence of low-level cyclonic vorticity in the lee of a mountain ridge before the period of rapid development ensues. The present study provides a mechanism that produces vorticity and divergence fields that could be necessary precursors to the formation of lee cyclones. An association between deformation flows incident on the Alps and lee cyclogenesis has not been established; however, such an association cannot be ruled out. An example, shown in Fig. 1b, displays the pressure pattern that preceded the major lee cyclogenesis event of 3–4 March 1982 (Buzzi and Tosi 1982). In this case, the deformation flow appears to be present as a consequence of the upstream pressure pattern, and the tendency to circumvent the ridge does not appear to represent an Alpine blocking phenomenon.

A natural extension of the present work would be to follow the subsequent time development that arises from the use of the steady state model solutions as initial conditions. In particular, the interaction of the low-level lee vortex with an approaching baroclinic wave, characterized by a nonuniform potential vorticity distribution, may clarify the physical processes that are important in the formative stages of deep lee cyclones. If this particular process proves to be relatively important, numerical prediction models may fail to forecast lee cyclogenesis unless the model resolutions are sufficient to capture the initial development of low-level cyclonic vorticity.

Acknowledgments. Financial support for this investigation was provided by the National Science Foundation under NSF Grants ATM 86-08333 and ATM 86-17636. The numerical computations were carried out on the Pyramid 90X supermini computer at the University of Colorado Center for Atmospheric Theory and Analysis. One author (W.B.) expresses his thanks to Olivera Haney, who provided computational assistance during the early stages of this research, carried out at the Naval Postgraduate School.

APPENDIX

Evaluation of Approximations

1. The quadratic terms in (5)

It has been shown in I that the quadratic terms neglected in (5) represent relatively small corrections to the mountain vortex solution if the nondimensional mountain height satisfies $\epsilon/D \leqslant 0.5$ and $\mathrm{Ro} \leqslant 0.3$. The quadratic terms associated with the basic current are of order α^2, while the terms retained in (5) are of order $\alpha \leqslant 0.2$. The neglect of the quadratic terms introduces a small error of the same magnitude in both the vortex solution and the basic current.

2. The geostrophic momentum approximation

The divergence theorem derived from the Boussinesq, hydrostatic, inviscid primitive equations is given by

$$\frac{Dd}{Dt} = \frac{\zeta^2 - \gamma^2 - d^2}{2} + \zeta_a, \tag{A1}$$

where the vertical velocity has been neglected (Petterssen 1953). This theorem derived under the geostrophic momentum approximation is given by (35):

$$0 = \frac{\zeta_g^2 - \gamma_g^2 + \zeta_g\zeta_a - \tau_g\tau_a - \eta_g\eta_a}{2} + \zeta_a, \tag{A2}$$

where the geostrophic divergence is identically zero. The validity of the geostrophic momentum approximation may be estimated by comparing the terms in (A1) that are absent in (A2), with those that are retained in (A2). In particular, the geostrophic momentum approximation is valid if

$$\frac{|\zeta_a|^2}{2}, \frac{|\gamma_a|^2}{2}, \frac{|d_a|^2}{2}, \frac{Dd_a}{Dt} \ll \zeta_a. \tag{A3}$$

These conditions will be satisfied by (35)–(38) if $\epsilon/D \leqslant 0.5$, $\alpha \leqslant 0.2$, and $\mathrm{Ro} \leqslant 0.3$. These upper limits are the parameter values employed in the present study. Clearly, the criteria (A3) for the validity of the geostrophic momentum approximation cannot be satisfied where ζ_a is small. In general, however, the geostrophic momentum approximation is considered valid if *typ-*

ical magnitudes of the ageostrophic quantities in the flow field satisfy (A3). In particular, (A3) is satisfied in the lee of the mountain, where the cyclonic vorticity and convergence are the predominant features in the flow.

REFERENCES

Blumen, W., and B. D. Gross, 1987: Semigeostrophic flow over orography in a stratified rotating atmosphere. Part I: Steady three-dimensional solutions over finite ridges. *J. Atmos. Sci.*, **44,** 3007–3019.

Buzzi, A., and E. Tosi, 1982: Lee cyclogenesis during the ALPEX SOP. *ALPEX Preliminary Scientific Results,* WMO Geneva, GARP-ALPEX No. 7, 41–48. [Available from the Secretariat of the WMO, C.P. No. 5. CH-1211 Geneva 20, Switzerland]

Hoskins, B. J., 1975: The geostrophic momentum approximation and the semi-geostrophic equations. *J. Atmos. Sci.*, **32,** 233–242.

Huppert, H. E., and K. Bryan, 1976: Topgraphically generated eddies. *Deep Sea Res.*, **23,** 655–679.

McGinley, J., 1982: A diagnosis of Alpine lee cyclogenesis. *Mon. Wea. Rev.*, **110,** 1271–1287.

Merkine, L. O., and E. Kálnay-Rivas, 1976: Rotating semigeostrophic flow over finite isolated topography. *J. Atmos. Sci.*, **33,** 908–922.

Petterssen, S., 1953: On the relation between vorticity, deformation, and divergence and the configuration of the pressure field. *Tellus,* **5,** 231–237.

Radinović, D., 1986: On the development of orographic cyclones. *Quart. J. Roy. Meteor. Soc.*, **112,** 927–951.

Sherman, L., 1952: On the scalar-vorticity and horizontal-divergence equations. *J. Meteor.*, **9,** 359–366.

Smith, R. B., 1979: Some aspects of quasigeostrophic flow over mountains. *J. Atmos. Sci.*, **36,** 2385–2393.